Ultrasound Imaging Enables Longitudinal Tracking of Vascular Changes that Correlate with Immune Cell Infiltration After Radiotherapy

Shannon E. Martello[1], Jixin Xia[2], Jiro Kusunose[3], Benjamin C. Hacker[1], McKenzie A. Mayeaux[2], Erica J. Lin[4], Adrienne Hawkes[3], Aparna Singh[3], Charles F. Caskey[3], Marjan Rafat[1,2,5]*

[1]Department of Chemical and Biomolecular Engineering, Vanderbilt University, Nashville, TN, USA

[2] Department of Biomedical Engineering, Vanderbilt University, Nashville, TN, USA

[3] Department of Radiology, Vanderbilt University Medical Center, Nashville, TN, USA

[4] Department of Biological Sciences, Vanderbilt University, Nashville, TN, USA

[5]Department of Radiation Oncology, Vanderbilt University Medical Center, Nashville, TN, USA

*Author for correspondence: Marjan Rafat, PhD, Engineering and Science Building, Rm. 426, Vanderbilt University, Nashville, TN 37212. Phone: (615) 343-3389, Fax: (615) 343-7951, E-mail: marjan.rafat@vanderbilt.edu

Abstract

While immunotherapy shows great promise in patients with triple negative breast cancer, many will not respond to treatment, and predicting response is made difficult by significant tumor heterogeneity. Non-invasive imaging of the tumor vasculature enables the monitoring of treatment and has potential to aid in predicting therapeutic response. Here, we use ultrafast power doppler ultrasound (US) to track longitudinal changes in the vascular response to radiotherapy in two breast cancer models to correlate vascular and immune changes in the tumor microenvironment. Tumor volume and vascular index were calculated to evaluate the effects of radiation using US imaging. US tumor measurements and the quantified vascular response to radiation were confirmed with caliper measurements and immunohistochemistry observations, respectively, demonstrating a proof-of-principle method for non-invasive vascular monitoring. Additionally, we found significant infiltration of CD8+ T cells into irradiated tumors 10 days after radiation, which followed a sustained decline in vascular index that was first observed 1 day post-radiation. Taken together, our findings reveal the potential for ultrafast power doppler US to evaluate changes in tumor vasculature that may be indicative of the tumor-immune microenvironment and ultimately improve patient outcomes by predicting response to immunotherapy.

Keywords:

Ultrasound; Radiotherapy; vasculature; triple negative breast cancer; immune response; immunotherapy

Introduction

The incidence of breast cancer is rising, with over 300,000 new diagnoses annually (1). Approximately 15% of cases are identified as triple negative breast cancer (TNBC), which is characterized by a disproportionally high death rate due to its aggressive nature and lack of non-targeted therapies (2, 3). Radiotherapy (RT) is a mainstay of TNBC treatment and significantly reduces the risk of recurrence after surgery (4–6). RT exerts biological effects beyond tumor cell killing on both short- and long-term scales, altering physical and molecular vascular characteristics and influencing immune cell infiltration and phenotype (7–9). Recently, it has been suggested that RT can be used as a tool to elicit immune cell infiltration and activation in the tumor, thereby improving the efficacy of immunotherapies in otherwise immunologically “cold” tumors (10–12). While some TNBC patients respond well to immunotherapies like immune-checkpoint blockade (13–15), it remains difficult to predict therapeutic outcomes due to varying degrees of malignancy, immune landscape, and general tumor heterogeneity across patients.

The tumor vasculature can influence the therapeutic response molecularly and physically by controlling immune cell trafficking, anti-tumor immunity, and drug delivery. Changes in microvascular structure are indicative of tumor progression and have been implicated in predicting response to RT (16–18). Recent work has also linked vascular changes in skin tumors with immune cell infiltrate and response to immunotherapy, demonstrating a critical connection between tumor vasculature and the immune system (19). Non-invasive monitoring of the tumor vascular response to RT could therefore potentially be used to predict response to immunotherapy.

Previous studies used contrast-enhanced ultrasound (US) to differentiate vessel sizes and measure fibrosarcoma response to radiation (18, 20) and high frequency power doppler US to monitor breast tumor response to RT and anti-angiogenic therapy (21). Here, we use ultrafast power doppler US to measure longitudinal changes in tumor vasculature. Ultrafast US combines

improved resolution and sensitivity, allowing for deeper penetration of tissues and more accurate reconstruction of vascular changes over time (22, 23). In this study, ultrafast US images were taken at multiple timepoints following tumor irradiation in two TNBC models with varying degrees of malignancy to investigate differences in vascular response to RT and correlate these responses with local changes in immune cell populations. We found that vascular responses to RT determined by US imaging correspond with histological staining and that changes in vascularity precede changes to the local immune response. Thus, ultrafast power doppler US may be used to predict changes in the immune microenvironment and determine timepoints for delivery of adjuvant immunotherapy.

Methods

Radiation

Animal studies were performed in accordance with the institutional guidelines and protocols approved by the Vanderbilt University Institutional Animal Care and Use Committee. Female BALB/c mice (8-10 weeks old) were inoculated with $5x10^4$ $4T1^{luc}$ (4T1) or $1x10^6$ 67NR murine TNBC cells. Tumor length and width were measured using digital calipers (Fisher Scientific) beginning one (4T1) or two (67NR) weeks post-inoculation. Tumor volume was estimated by volume=$(L_1^2xL_2)/2$, where L_1 is the smallest and L_2 is the largest measurement of the tumor. At 100 mm^3, tumors were irradiated to 12 Gy using a 300kVp cabinet x-ray system filtered with 0.5 mm Cu. Mice were anesthetized with 2.5% isoflurane and shielded using a 2 cm thick Cerrobend shield with 1 cm wide and 1.5 cm long apertures to expose the tumors. Transmission through the shield was less than 1%.

US Imaging Protocol

Animals were anesthetized with 1.5-2% isoflurane. An imaging array (L12-5, Philips, Reedsville, PA) was acoustically coupled to the palpable tumor target through a 6 cm tall cavity filled with

warm degassed water. A Verasonics Vantage Ultrasound system (Verasonics Inc, Kirkland, WA, USA) was used for imaging planning and acquisition. Real-time B-mode and power doppler imaging were used to check coupling quality, locate tumor center, and identify the spatial extent of the tumor in the elevational direction. Microbubbles were injected via retro orbital injection and 6-12 image planes were acquired with 1-mm spacing to capture a volumetric image of the tumor. For each plane, 5100 frames of radio frequency (RF) data were acquired at frame rate of 510 Hz at 8.9 MHz. Each frame was comprised of 3 angled compounding planes ranging from -18° to 18°. The acquired RF data was reconstructed offline to IQ data.

US offline processing

Motion correction was performed every 30 frames. The mean of each frame was taken and normalized by the 30 frames median. Standard deviation of 15 frames with low mean amplitude was used to calculate a stability threshold. Outlier frames that exceeded the threshold were replaced with linear interpolation from the remaining frames (24). The motion corrected IQ data was then passed through an SVD filter with 5% cutoff, a Butterworth bandpass filter from 25 Hz to 125 Hz, and a Top-hat filter with 2 mm disk size to help remove static tissue signal and enhance moving signals that depicts vasculature. The filtered data was then summed to produce a power doppler image. The summed power doppler images was passed through Frangi filter which enhanced tubular structures (25). The tumor region was manually segmented from power doppler images overlayed on the corresponding B-mode images using MATLAB ginput function (The MathWorks, Inc., Natick, Massachusetts, US). Total tumor volume was evaluated by summing the volume for each acquired plane. The dimmest vessel region on the Frangi filtered image was selected manually with MATLAB ginput and a brightness threshold was calculated taking the mean of the selected region. A binary mask was generated using the brightness threshold, segmenting the vasculature within the tumor. The total vasculature volume was calculated from

the number of voxels in the masks across the planes. The vascular index was the ratio of the total vasculature volume to the total tumor volume.

Histological analysis

At 1 or 10 days post-RT, tumors were resected and placed in 10% neutral buffered formalin (NBF) for 24 h at 4ºC and then in 70% ethanol until embedding in paraffin. Sections (4 µm) were deparaffinized, rehydrated, and boiled in citric acid (10 mM pH 6) for antigen retrieval. For immunofluorescence, blocking in 10% donkey serum was followed by overnight incubation at 4ºC with anti-CD31 (1:100; R&D Systems) and subsequent incubation with a fluorescent secondary antibody. An autofluorescence quenching solution (Vector Laboratories) was used to quench autofluorescence before nuclear staining with 4',6-diamidino-2-phenylindole dihydrochloride. All samples were imaged using an inverted Leica microscope (DMi8). ImageJ was used to quantify percent area of positive CD31 staining.

Flow Cytometry

At 1 or 10 days post-RT, tumors, spleens, and lungs were resected and minced in serum-free RPMI media. Tumors and lungs were then placed in a 400 µg/mL DNase and 20 µg/mL Liberase digestion solution and incubated for 30 minutes in a 37ºC water bath. Digestion was stopped by adding RPMI + 10% fetal bovine serum. Lungs and spleens were then incubated in ACK lysis buffer for 2 minutes before adding 3% FBS in PBS to halt lysis. All cells were stained with Aqua fixable viability stain (ThermoFisher) and FC receptors were blocked with CD16/32 (Biolegend) while simultaneously staining for all surface markers. Cells were incubated for 20 minutes at 4ºC, rinsed with PBS, and fixed with 1% NBF for at least 20 minutes at 4ºC. Flow cytometry was performed on a four-laser Amnis CellStream machine (Luminex) and FlowJo software (Becton Dickinson) was used for analysis. The following antibody clones were used for analysis: CD45

(30-F11), CD11b (M1/70), F4/80 (BM8), Ly6G (1A8), GR-1 (RB6-8C5), MHCII (M5/114.15.2), CD11c (N418), CD3 (17A2), CD4 (GK1.5), and CD8 (53-6.7).

Statistical Analysis

To determine statistical significance, differences in CD31 expression and in immune cell populations after radiation and between the two tumor types were determined by two-way ANOVA. Student's unpaired t-tests were used to determine statistical significance between timepoints for each condition and between conditions at each timepoint. All statistical analyses were performed in GraphPad Prism 10.

Results

US tracks differences in tumor volume and vascularity over time

To determine whether ultrafast US can non-invasively monitor tumor response to RT and distinguish differences in malignancy, metastatic 4T1 and non-metastatic 67NR tumors were irradiated to 12 Gy—a non-curative dose that allowed us to study both vascular and immune cell changes over time. At 1 day prior to and 1 and 8 days after RT, tumor volume was quantified using B-mode US, and vascularity was quantified using high frame rate doppler US (**Figure 1A**) to determine feasibility of visualizing changes on both short and long timescales. US-derived volumes measurements were largely in agreement with manual caliper measurements in both 67NR and 4T1 tumor models (**Figure 1B**). 67NR tumors exhibited a marked stall in growth post-RT, while the highly metastatic 4T1 tumors were unaffected. Accuracy of the US volume measurements compared to caliper measurements highlights the potential of this techniques to provide a more quantitative and less subjective method for tracking size changes over time post-RT.

Noticeable differences in vascularity between the tumor types and after RT were also observed in US analysis. Vascular index of each tumor was derived from Frangi filtered images and

normalized to the measured tumor volume, enabling non-invasive quantification of vascular changes that are independent of tumor size. US images showed that the 67NR tumors were highly vascular, with clear vessels throughout the tumor both before and after radiation (**Figure 2A**). Conversely, 4T1 tumors appeared largely avascular throughout the center of the mass and visualization of vascular networks was difficult, potentially indicating a necrotic core. At 1 day post-RT, 67NR tumors showed a significant decrease in vascular index from 0.17 ± 0.04 to 0.13 ± 0.04 that did not recover up to 1 week later (**Figure 2B**). Control mice bearing 67NR tumors showed a 35% increase from 0.17 ± 0.08 to 0.23 ± 0.17 at 8d post-RT. There were no significant changes in vascular index in the 4T1 tumors in both irradiated and control mice (**Figure 2C**), likely due to reduced vascularity within the tumor at early time points.

Image-derived vascular index correlates with histological analysis

Immunofluorescence staining for CD31 was performed on control and irradiated 67NR and 4T1 tumors to validate the findings of US imaging and compare it to standard practices of quantifying vascular changes in both pre-clinical and clinical studies. 67NR tumors were characterized by large numbers of small vessels compared to 4T1 tumors, which displayed large areas of necrosis and larger, more disorganized vessels (**Figure 3A**). After RT, 67NR tumors showed a slight decrease in CD31 expression compared to control tumors, and this persisted up to 10 days post-RT, at which point irradiated tumors had significantly reduced CD31+ vessels (**Figure 3B**). 4T1 tumors showed no significant differences over time or after irradiation (**Figure 3C**). These observations corroborate the trends observed using US imaging, further underscoring the feasibility of using US to identify and monitor vascular changes non-invasively over time.

Radiotherapy elicits an increase in CD8:CD4 T cell ratios that follows vascular changes

We next sought to determine whether our non-curative dose of RT could produce an immune response that correlated with the vascular changes we observed using US imaging. Flow

cytometry analysis of tumor-infiltrating myeloid and lymphocyte populations was performed at 1 and 10 days post-RT to identify early and late responses. In both tumor types, we did not see any significant changes in immune cell populations at 1 day post-RT. However, both 67NR and 4T1 tumors showed significantly higher populations of CD45+ immune cells at 10 days post-RT (**Figure 4A, B**). 67NR tumors showed a significant increase in T cells that likely drove the increase in general immune cells (**Figure 4A**). In 4T1 tumors, controls showed a significant, though less pronounced, increase in immune cells at 10 days, likely due to tumor growth and inflammation associated with this tumor (**Figure 4B**). In contrast to 67NR tumors, the increase in general immune cell infiltration appeared to be driven by significant increases in CD11b+ myeloid cells, potentially indicating an immunosuppressive environment that was exacerbated by RT. Analysis of T cell subpopulations showed increased CD4+ cells in both control and irradiated 67NR tumors, but an increase in CD8+ T cells only in irradiated tumors**,** causing a nearly three-fold increase in the ratio of CD8:CD4 T cells in these tumors (**Figure 4C**). This demonstrates the potentially immunostimulatory nature of this radiation scheme. Subpopulations of T cells and the ratio of CD8:CD4 T cells were unaffected by radiation or time in 4T1 tumors (**Figure 4D**), highlighting the expected differences in the immune landscapes between 67NR and 4T1 tumors. The change in immune and CD8+ T cell infiltration of irradiated 67NR tumors at 10 days post-RT correlated with the observed decrease in vascularity beginning as early as 1 day post-RT, suggesting the utility of non-invasive vascular monitoring with prediction of immune responses to RT.

Discussion

In this proof-of-principle study, we used ultrafast power doppler US imaging to track longitudinal, RT-induced vascular changes in two tumor models that differ in malignancy. This technique was able to non-invasively monitor post-RT vascular changes that correspond to changes observed via histological analysis. Moreover, the decrease in vascular index observed via US at 1 day post-RT in 67NR mice preceded a significant increase in the CD8+ cytotoxic T cell population that was

only observed in irradiated mice (**Figure 4**). Previous work has found the vasculature of 67NR tumors to be substantially different from 4T1 tumors, which was corroborated by our study (26, 27). The slower growing 67NR tumors have time to form more complete vessels with a thicker endothelium compared to the 4T1 tumors, which are characterized by leaky, tortuous vasculature and large areas of necrosis. Based on our observations, it is possible that RT caused damage to the mostly intact 67NR vessels at 1 day post-RT that was sustained up to 10 days, enabling easier infiltration of immune cells. Because 4T1 tumors are immunologically cold and highly aggressive, a higher dose of RT may be necessary to elicit vascular changes and impact immune cell infiltration. Ultimately, the change in response to RT of 67NR vasculature that was observed using non-invasive imaging could be predictive of immune cell infiltration and response to therapy as we observed substantial vascular changes after 1 day but no immune cell changes until up to 10 days post-RT. A recent study correlated high vascularity with high inflammation in basal cell carcinomas to predict therapeutic outcomes (19), further underscoring this concept.

Identifying methods that accurately monitor changes in tumor vasculature after RT may be critical for predicting response to adjuvant immunotherapy and determining outcomes. Future experiments will provide more in depth characterization of vascular changes using US and further link changes in tumor vasculature to changes in tumor-infiltrating immune cell populations. Taken together, this work demonstrates the potential for US imaging to monitor changes in response to RT that may be predictive of shifts in the immune landscape of the tumor, ultimately improving outcomes and responses to immunotherapy.

Acknowledgements

The authors thank Dr. Michael Freeman for irradiator use and Dr. Austin Kirschner and the radiation physics staff for constructing the Cerrobend shield. We also thank the Vanderbilt Translational Pathology Shared Resource (TPSR) for tissue sample preparation. This research

was financially supported by the Focused Ultrasound Foundation Cancer Immunotherapy Award, NIH grant #R00CA201304, and P30CA068485 (TPSR).

References

1. Siegel RL, Miller KD, Sandeep N, *et al.* Cancer statistics, 2023. *CA. Cancer J. Clin.* 2023;73:17–48.

2. Zagami P, Carey LA. Triple negative breast cancer: Pitfalls and progress. *npj Breast Cancer 2022 81*. 2022;8:1–10.

3. Baranova A, Krasnoselskyi M, Starikov V, *et al.* Triple-negative breast cancer: current treatment strategies and factors of negative prognosis. *J. Med. Life*. 2022;15:153–161.

4. Lowery AJ, Kell MR, Glynn RW, *et al.* Locoregional recurrence after breast cancer surgery: A systematic review by receptor phenotype. *Breast Cancer Res. Treat.* 2012;133:831–841.

5. Dragun AE, Pan J, Rai SN, *et al.* Locoregional recurrence in patients with triple-negative breast cancer: preliminary results of a single institution study. *Am. J. Clin. Oncol.* 2011;34:231–237.

6. Afghahi A, Purington N, Han SS, *et al.* Higher Absolute Lymphocyte Counts Predict Lower Mortality from Early-Stage Triple-Negative Breast Cancer. *Clin. Cancer Res.* 2018;24:2851–2858.

7. Choi SH, Kim AR, Nam JK, *et al.* Tumour-vasculature development via endothelial-to-mesenchymal transition after radiotherapy controls CD44v6+ cancer cell and macrophage polarization. *Nat. Commun. 2018 91*. 2018;9:1–18.

8. Vanpouille-Box C, Alard A, Aryankalayil MJ, *et al.* DNA exonuclease Trex1 regulates radiotherapy-induced tumour immunogenicity. *Nat. Commun.* 2017;8:15618.

9. Bouchet A, Serduc R, Laissue JA, *et al.* Effects of microbeam radiation therapy on normal and tumoral blood vessels. *Phys. Medica*. 2015;31:634–641.

10. Wang Y, Liu ZG, Yuan H, *et al.* The reciprocity between radiotherapy and cancer immunotherapy. *Clin. Cancer Res.* 2019;25:1709–1717.

11. Galluzzi L, Aryankalayil MJ, Coleman CN, *et al.* Emerging evidence for adapting radiotherapy to immunotherapy. *Nat. Rev. Clin. Oncol. 2023*. 2023:1–15.

12. Aguilera TA, Elghonaimy EA, Shehade H, *et al.* Induced Tumor Heterogeneity Reveals Factors Informing Radiation and Immunotherapy Combinations. *Clin. Cancer Res.* 2020;26:2972–2985.

13. Cyprian FS, Akhtar S, Gatalica Z, *et al.* Targeted immunotherapy with a checkpoint inhibitor in combination with chemotherapy: A new clinical paradigm in the treatment of triple-negative breast cancer. *Bosn. J. Basic Med. Sci.* 2019;19:227.

14. Emens LA, Adams S, Barrios CH, *et al.* First-line atezolizumab plus nab-paclitaxel for unresectable, locally advanced, or metastatic triple-negative breast cancer: IMpassion130 final overall survival analysis. *Ann. Oncol. Off. J. Eur. Soc. Med. Oncol.* 2021;32:983–993.

15. Cortes J, Cescon DW, Rugo HS, *et al.* Pembrolizumab plus chemotherapy versus placebo plus chemotherapy for previously untreated locally recurrent inoperable or metastatic triple-negative breast cancer (KEYNOTE-355): a randomised, placebo-controlled, double-blind, phase 3 clinical trial. *Lancet (London, England)*. 2020;396:1817–1828.

16. Gessner RC, Aylward SR, Dayton PA. Mapping Microvasculature with Acoustic Angiography Yields Quantifiable Differences between Healthy and Tumor-bearing Tissue Volumes in a Rodent Model. *https://doi.org/10.1148/radiol.12112000*. 2012;264:733–740.

17. Ribatti D, Nico B, Ruggieri S, *et al.* Angiogenesis and Antiangiogenesis in Triple-Negative Breast cancer. *Transl. Oncol.* 2016;9:453–457.

18. Kasoji SK, Rivera JN, Gessner RC, *et al.* Early Assessment of Tumor Response to Radiation Therapy using High-Resolution Quantitative Microvascular Ultrasound Imaging. *Theranostics*. 2018;8:156.

19. Sahu A, Kose K, Kraehenbuehl L, *et al.* In vivo tumor immune microenvironment phenotypes correlate with inflammation and vasculature to predict immunotherapy response. *Nat. Commun. 2022 131*. 2022;13:1–19.

20. Butler M, Perperidis A, Zahra JLM, *et al.* Differentiation of Vascular Characteristics Using Contrast-Enhanced Ultrasound Imaging. *Ultrasound Med. Biol.* 2019;45:2444–2455.

21. El Kaffas A, Giles A, Czarnota GJ. Dose-dependent response of tumor vasculature to radiation therapy in combination with Sunitinib depicted by three-dimensional high-frequency power Doppler ultrasound. *Angiogenesis*. 2013;16:443–454.

22. Errico C, Pierre J, Pezet S, *et al.* Ultrafast ultrasound localization microscopy for deep super-resolution vascular imaging. *Nat. 2015 5277579*. 2015;527:499–502.

23. Demené C, Payen T, Dizeux A, *et al.* 3-D Longitudinal Imaging of Tumor Angiogenesis in Mice in Vivo Using Ultrafast Doppler Tomography. *Ultrasound Med. Biol.* 2019;45:1284–1296.

24. Mace E, Montaldo G, Osmanski BF, *et al.* Functional ultrasound imaging of the brain: theory and basic principles. *IEEE Trans. Ultrason. Ferroelectr. Freq. Control*. 2013;60:492–506.

25. Kroon D-J. Hessian based Frangi Vesselness filter - File Exchange - MATLAB Central. *MATLAB Cent. File Exch.* 2023.

26. Papiernik D, Urbaniak A, Kłopotowska D, *et al.* Retinol-Binding Protein 4 Accelerates Metastatic Spread and Increases Impairment of Blood Flow in Mouse Mammary Gland Tumors. *Cancers 2020, Vol. 12, Page 623*. 2020;12:623.

27. Gerwing M, Hoffmann E, Kronenberg K, *et al.* Multiparametric MRI enables for differentiation of different degrees of malignancy in two murine models of breast cancer. *Front. Oncol.* 2022;12:1000036.

Figures

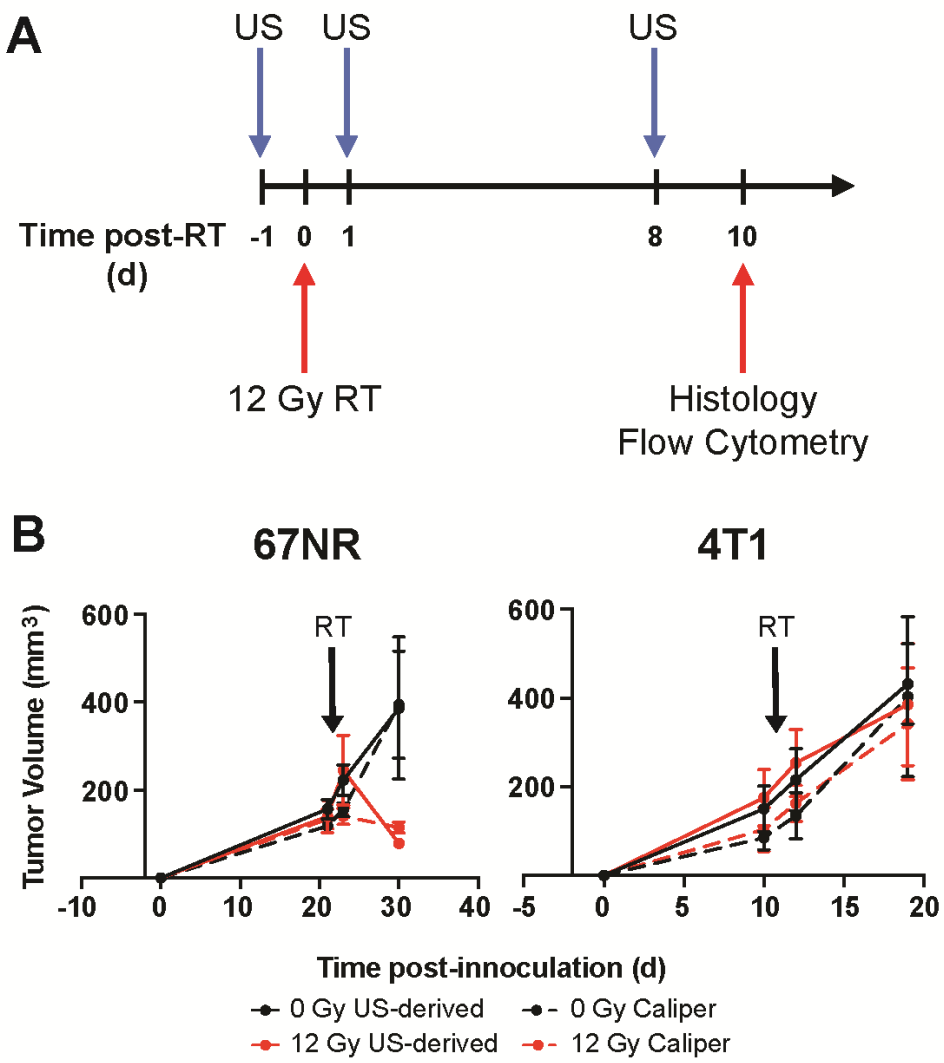

Figure 1. Ultrasound (US) imaging accurately tracks changes in tumor volume post-RT. A. Experimental timeline. 4T1 and 67NR tumors were irradiated to 12 Gy. US imaging was performed 1 day prior to and 1 and 8 days after RT. Tumors were resected at 10 days post-RT for histological and flow cytometric analysis. **B.** Tumor volumes measured via US at -1, 1, and 8 days post-RT compared to manual caliper measurements taken at the same timepoints for 67NR and 4T1 tumors. Error bars show standard error with n=13-15 mice per condition.

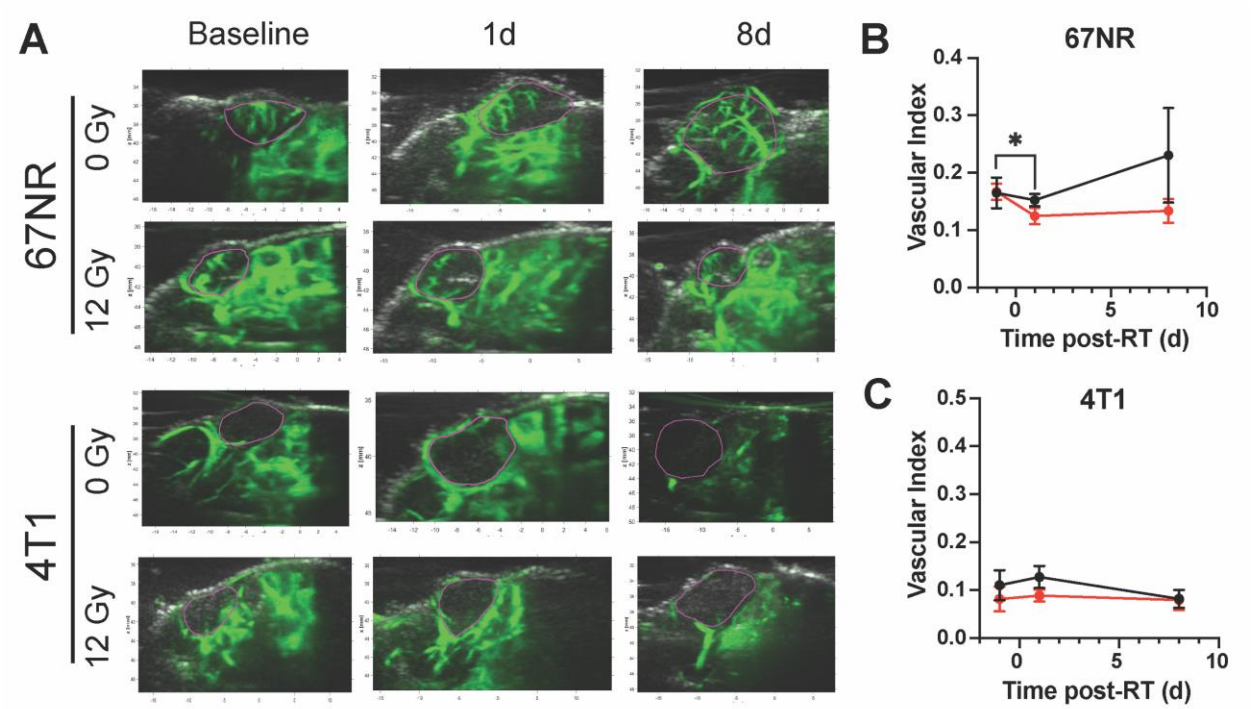

Figure 2. Ultrafast US imaging quantifies vascular changes post-RT. A. Representative images of power doppler images of vascular structure overlaid onto B-mode images of the tumor. Vascular structures imaged with doppler are shown in green. Circular selections indicate the identified tumor volumes. Quantification of the vascular volume from doppler images and tumor volume from B-mode images enabled calculation of vascular index post-RT over time in **B.** 67NR (n = 9 for -1 and 1 d; n = 4 for 8 d) and **C.** 4T1 (n = 13 for -1 and 1d and n = 7 for 10 d 0 Gy; and n = 15 for -1 and 1 d and n = 10 for 10 d 12 Gy) tumors. Error bars represent standard error with *p<0.05 determined by student's t-test between timepoints.

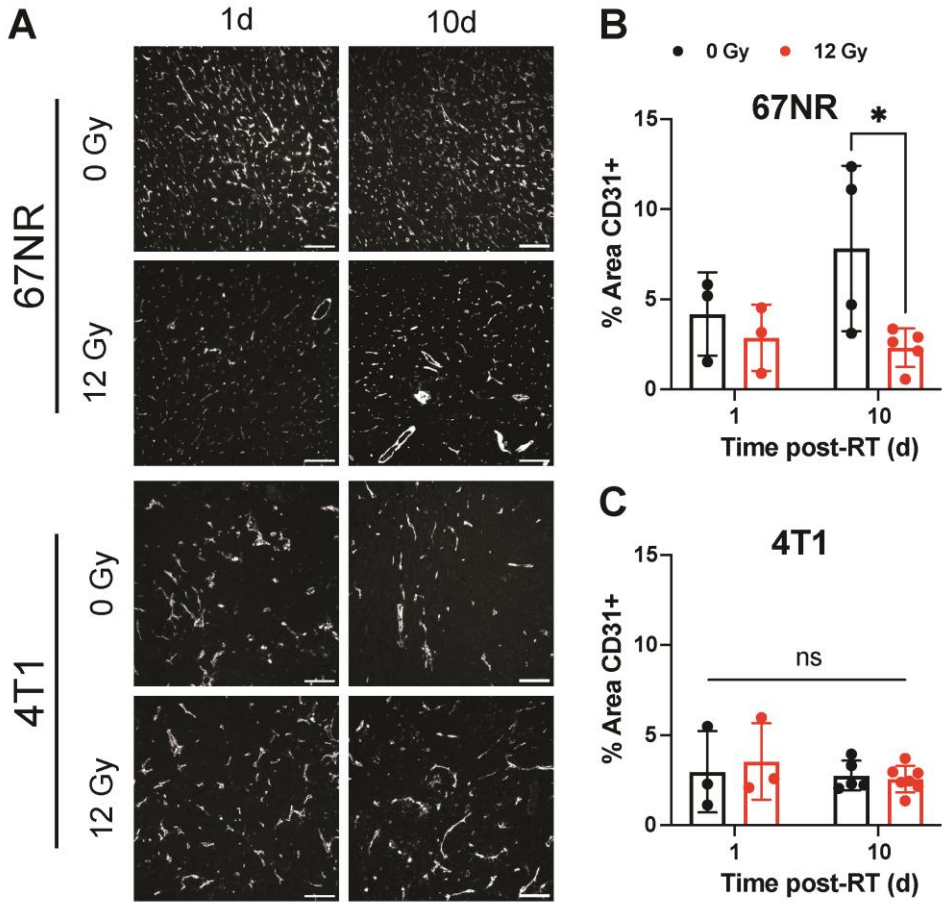

Figure 3. Histology shows vascular differences after radiation and between tumor types that correspond to US measurements. A. Representative CD31 immunofluorescence staining of control and irradiated 67NR and 4T1 tumors at 1 and 10 days post-RT. Scale bar is 100 µm. Quantification of the percent area of positive CD31 staining per field of view in **B.** 67NR and **C.** 4T1 tumors (n = 3-7 mice per condition). Error bars represent standard error with *$p<0.05$ as determined by two-way ANOVA.

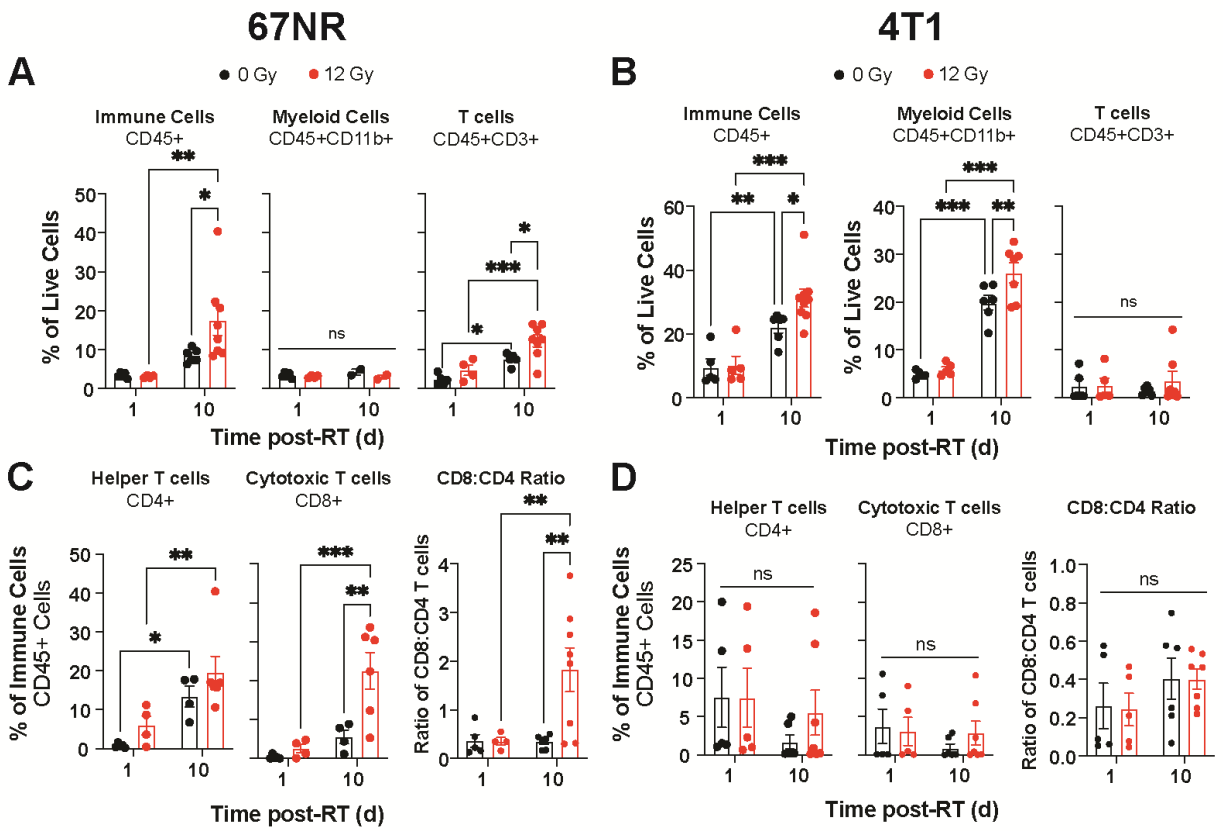

Figure 4. Immune cell infiltration post-RT differs between 67NR and 4T1 tumors. Flow cytometry characterization of tumor-infiltrating immune cell populations at 1 and 10 days post-RT, including general CD45+ immune cells, CD11b+ myeloid cells, and CD3+ T lymphocytes in **A.** 67NR and **B.** 4T1 tumors (n = 4-15 mice per condition). Further characterization of T lymphocyte subsets, including CD4+ helper T cells, CD8+ cytotoxic T cells, and the ratio of CD8:CD4 T cells in **C.** 67NR and **D.** 4T1 tumors. Ratios calculated from absolute counts of CD45+CD3+CD4+ and CD45+CD3+CD8+ cells in each tumor. Error bars represent standard error with *p<0.05, **p<0.01, and ***p<0.001 as determined by two-way ANOVA.